Turkish Journal of Electrical Engineering & Computer Sciences

http://journals.tubitak.gov.tr/elektrik/

Research Article

Turk J Elec Eng & Comp Sci
(2016) 24: 4751 – 4762

doi:10.3906/elk-1408-82

Double bow-tie FSS for X-band and K$_u$-band operations with its parametric analyses

Selma ÇİĞDEM, Cihan TUNCA, Sultan CAN*, Asım Egemen YILMAZ
Department of Electrical and Electronics Engineering, Ankara University, Ankara, Turkey

Received: 14.08.2014 • **Accepted/Published Online:** 09.09.2015 • **Final Version:** 06.12.2016

Abstract: This paper demonstrates double bow-tie frequency selective surface (FSS) geometry for X-band applications with a bandwidth value of 1.82 GHz and K$_u$-band applications with a bandwidth value of 3.44 GHz. Throughout this study, parametric analyses of the proposed structure are also performed. Alterations in the reflection and transmission characteristics of this specially designed structure by virtue of defined variables are analyzed. Those variables are determined by considering the geometric and material properties of the proposed structure. To analyze the reflection and transmission coefficients, two different simulators, namely the High Frequency Structure Simulator (ANSYS HFSS), which is based on the finite element method (FEM), and the Computer Simulation Technology Studio Suite (CST Studio Suite), which is based on the finite integration method (FIM), are used. The structure is validated via those two solvers. Good agreement is obtained by both solvers, and the results are compared in terms of frequency, return loss, insertion loss, and fractional bandwidth.

Key words: Frequency selective surface, double bow-tie FSS, K$_u$-band, X-band

1. Introduction

The development in both science and technology is actually a simple example of mutuality. When science states a rule, not necessarily but usually, it is applied to technology, so that the number of applications increases accordingly. Wireless communication is one of the examples that the theory reached a level of maturity as well as the application areas especially in the microwave branch. Radar systems, antenna design, and broadband communication are examples for those areas [1–13]. Due to the development in microwave technology, various forms of electromagnetic waves with different frequencies are used to communicate, which causes several problems resulting from the interference of electromagnetic waves, since those waves interact with each other and with the environment [1,2]. Especially for application areas requiring operation safety, high performance and stability in systems filtering electromagnetic waves appear to be one of the most important problems for engineers. In the literature, several periodic arrangements are used with different geometries as a way of filtering electromagnetic waves [1–4,10–13]. Periodically arranged surfaces, which are manufactured in order to use in blocking or passing a frequency band, can be excited by two different methods. The first one is passive grid arrays, which are excited via incoming electromagnetic waves. The second one is active grid arrays, which are excited by using a source for every individual unit cell. A frequency selective surface (FSS) is a passive array, which is a surface construction serving as a filter to incoming electromagnetic waves [2,10]. Reflection and transmission characteristics of a FSS depend on various factors, such as the material type,

*Correspondence: sultancan@ankara.edu.tr

layer thickness, polarization, and angle of incidence of incoming electromagnetic waves, dimensions, geometry, and periodicity of conducting material arranged on the substrate, etc. [10]. FSSs with angular-dependent behaviors are widely used in microwave, millimeter wave, and optic wave regimes of the spectrum, where they can act as either band-pass or band-stop filters [1,5,7,13]. Owing to several features, they are preferable since they increase the directivity, gain, and polarization purity of the received signals; in addition, bandwidth and frequency stabilization is possible by using these structures [11,12]. Due to their advantages, they are used in antenna radome design in order to prevent the interaction of electromagnetic waves and they are used in radar cross-section reduction by providing filtering [13]. Flexibility in the design process in terms of geometry and material made FSS much more attractive. Their geometry may be either planar or nonplanar. The planar ones are generally etched onto a dielectric layer and they consist of two main parts: dielectric substrate and the conducting patch.

This paper presents a double bow-tie planar FSS geometry for X-band and K_u-band applications. The effects of the geometric and material parameters are analyzed via a finite integration technique based CAD solver called Computer Simulation Technology (CST-Microwave Studio). The results of the parametric analysis are verified via a finite element method based solver called High Frequency Structure Simulation (ANSYS HFSS). Along with the variation in parameters, variations in corresponding bandwidth, resonance frequency, and gain are examined. Throughout the analyses, the conducting patch is specified to be copper with 35 mu m thickness. The electromagnetic wave that is radiating from the port is assumed to be at a normal incidence; however, in order to evaluate the polarization dependency, the electromagnetic wave radiating with different incidence angles is also considered in the following section.

2. Proposed FSS geometry and boundary conditions

The double bow-tie geometry proposed in this study is shown in Figure 1. The structure simply contains a substrate having a side length of w and a thickness of t_s, and a conducting patch consisting of two bow ties etched on the substrate. Both bow ties consist of two identical equilateral triangles with side lengths a with a copper thickness of t_c. The distance r denotes the length between the tip of the triangle and its centroid.

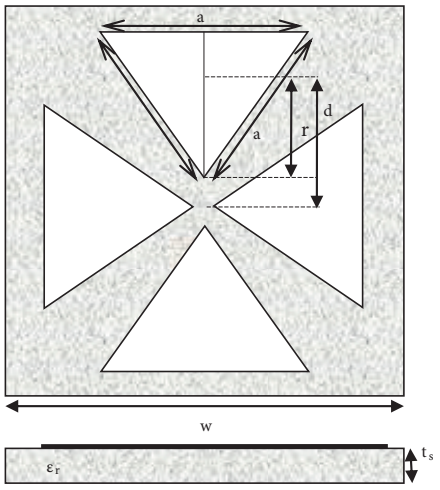

Figure 1. Proposed FSS geometry.

As seen in the proposed figure above the permittivity of the substrate is denoted as ε_r, and in the simulation software packages, the boundary condition is assigned as shown in Figure 2a. The front and back faces of the unit cell are assigned as the ports. In this manner, the structure is extended to infinity in both sides with double periodicity.

The excitation of the proposed structure is presented in Figure 2b. It should be noted that the direction of the propagation is perpendicular to the surface. The electromagnetic wave is assumed to radiating to the FSS structure at normal incidence. However, in the following sections the effect of incidence angle will also presented.

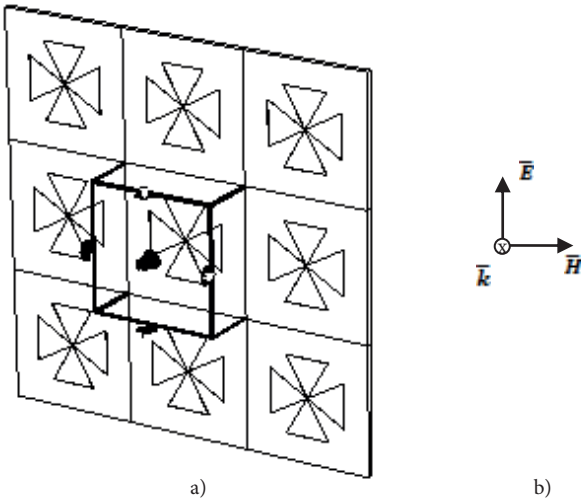

a) b)

Figure 2. a) Boundary conditions applied, b) Excitation throughout the simulations.

3. Parametric analysis of FSS geometry

The proposed geometry is evaluated by means of two different solvers. The scattering parameters are first analyzed via CST Microwave Studio and after that they are verified via HFFS. In order to analyze the proposed structure, two main parameters are considered: S_{11} and S_{21}, where the former corresponds to the reflection coefficient and the latter represents the insertion loss. By intuition, the parameters assumed to affect the electromagnetic characteristics of the geometry are nothing but the geometric and material properties. For this reason, the thickness of the substrate (t_s), the side length of the substrate (w), the distance of the tips of the triangles to the center of the substrate (d), the parameter denoting the height (physical size) of the triangles (r), and the permittivity value of the substrates (ε_r) are considered to be the parameters under investigation. It should be noted that all parameters are evaluated by ceteris paribus technique, by which only the evaluated parameter is modified while all other parameters are kept unchanged.

3.1. Impact of substrate side length (w) on S_{11} and S_{21}

A geometric parameter that affects the electromagnetic properties of the proposed structure is the side length of the substrate (w), which has a significant effect on the resonance frequency of the structure. The corresponding results of the evaluation are presented in Figure 3.

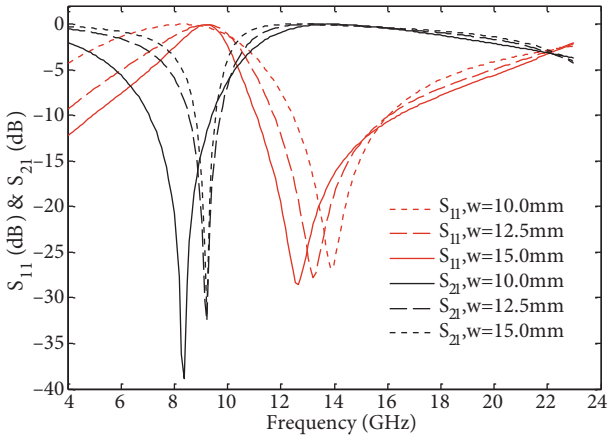

Figure 3. Impact of substrate side length (w) on a) S_{11} and b) S_{21} ($t_s = 0.70$ mm, $d = 3$ mm, $r = 3$ mm, $\varepsilon r = 3$ (Rogers 3003), $t_c = 0.035$ mm via CST).

An increment in the side length of the substrate causes a decrement in S_{11} resonance frequency value as seen in the results obtained from CST. The corresponding frequency values for 10 mm, 12.5 mm, and 15 mm are respectively 14.28 GHz, 13.29 GHz, and 12.99 GHz in CST; and 14.32 GHz, 13.46 GHz, and 12.78 GHz in HFSS with the same conditions. The return loss values vary between 26.4 dB and 28.12 dB for CST and between 26.02 dB and 28.19 dB in HFSS. The S_{21} resonance frequency value for CST increased from 8.73 GHz to 9.58 GHz with a 5 mm increment in the side length of the substrate. These increments caused a decrement in insertion loss with 10 dB. The S_{21} resonance frequency values obtained for side lengths of 10 mm, 12.5 mm, and 15 mm are 9.04 GHz, 9.64 GHz, and 9.5 GHz, respectively. The insertion loss values remained between 48.48 dB and 39.60 dB.

Fractional bandwidth (BW_f) was compared for varied w values and the results are presented in Table 1, which demonstrates lower frequency (f_l) and upper frequency (f_u) due to the –10 dB bandwidth, and center frequency (f_c) as well.

Table 1. Fractional bandwidth comparison for different ts values ($d = 3$ mm, $r = 3$ mm, $\varepsilon_r = 3$ (Rogers 3003), $t_c = 0.035$ mm).

	S_{11}				S_{21}			
w (mm)	f_l (GHz)	f_u(GHz)	f_c(GHz)	BW_f(%)	f_l(GHz)	f_u(GHz)	f_c (GHz)	BW_f(%)
10.00	12.46	16.01	13.88	25.58%	7.11	9.49	8.37	28.43%
12.50	11.75	16.07	13.20	32.73%	8.61	9.80	9.23	12.89%
15.00	11.10	16.47	12.55	42.79%	8.89	9.71	9.35	8.77%

The fractional bandwidth achieved was over 25% for S_{11} and over 8.7% for S_{21}.

3.2. Impact of substrate thickness (t_s) on S_{11} and S_{21}

In order to evaluate the impact of substrate thickness on resonance frequency, 3 different thickness values are determined and the proposed structure is again simulated via CST. The results are demonstrated in Figure 4a for S_{11} resonance and Figure 4b for S_{21} resonance. The corresponding resonance frequency values are 14.28 GHz, 13.07 GHz, and 12.25 GHz for the t_s values of 0.7 mm, 1.15 mm, and 1.6 mm, respectively for CST; 14.42 GHz, 13.25 GHz, and 12.68 GHz frequencies are observed for the mentioned thicknesses at HFSS. The return loss value varied between 14.68 dB and 26.43 dB for all simulation results. The differences between two

different solver based results are 0.14 GHz, 0.18 GHz, and 0.43 GHz for the thickness values of 0.7 mm, 1.15 mm, and 1.6 mm, respectively.

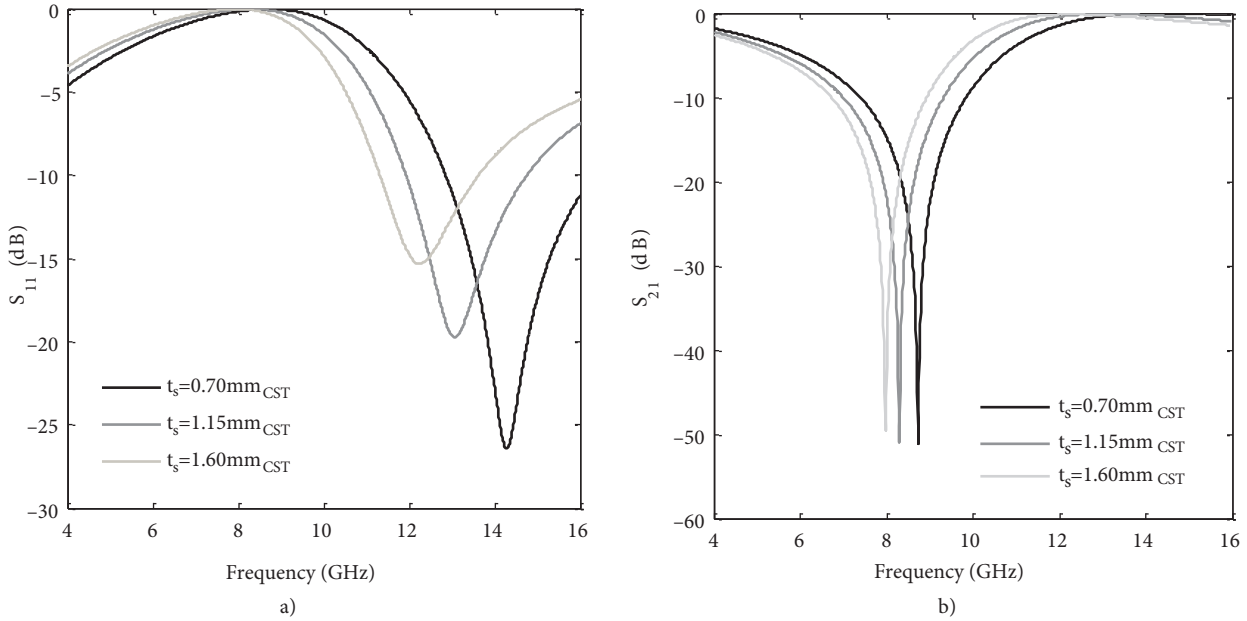

Figure 4. Impact of substrate side length (w) on a) S_{11} and b) S_{21} (t_s = 0.70 mm, d = 3 mm, r = 3 mm, ε_r = 3 (Rogers 3003), t_c = 0.035 mm via CST).

The increment in the value of t_s caused decrements in S_{21} resonance frequency value as well as the return loss value. As seen in Figure 4b, the insertion loss value decreased by 6.7 dB if the thickness value was increased by 0.45 mm when compared to a thickness value of 0.7 mm. Similarly, the insertion loss value decreased by 11.1 dB if the thickness value was increased by 0.9 mm when compared to a thickness value of 0.7 mm. For the thickness value of 0.7 mm, the frequency for S_{21} is evaluated as 8.73 GHz (CST) and 9.04 GHz (HFSS) with corresponding insertion loss values of 51.13 dB (CST) and 48.48 dB (HFSS), respectively. The increment in the thickness value by 0.45 mm caused a shift in S_{21} resonance frequency value by 0.44 GHz (via CST) and by 0.45 GHz (via HFSS). The frequencies for the thickness values of 1.6 mm are 7.98 GHz (CST) and 8.48 GHz (HFSS) with corresponding insertion losses of 49.59 dB (CST) and 48.22 dB (HFSS) as presented in Figure 4b. The S_{21} resonance frequency values increased with the decrement of the thickness concerning the CST results; however, there is a negligible exception for the value of t_s = 1.15 mm at HFSS. In addition, the decrement in the thickness caused an increment in the insertion loss value.

The comparison results are demonstrated in Table 2 in which the effect of ts value is evaluated with respect to the fractional bandwidth values.

Table 2. Fractional bandwidth comparison for different ts values (w = 10 mm, d = 3 mm, r = 3 mm, ε_r = 3 (Rogers 3003), t_c = 0.035 mm).

	S_{11}				S_{21}			
t_s(mm)	f_l (GHz)	f_u(GHz)	f_c(GHz)	BW_f(%)	f_l (GHz)	f_u(GHz)	f_c (GHz)	BW_f(%)
0.70	12.84	16.33	14.28	24.44	7.4	9.83	8.73	27.8
1.15	11.93	14.72	13.06	21.36	7.02	9.32	8.29	27.7
1.60	11.34	13.60	12.28	18.4	6.73	8.91	7.98	27.3

As seen in this table the fractional bandwidth for S_{11} decreases with the increment in t_s value as well as the bandwidth of the S_{21} bandwidth.

3.3. Impact of d on S_{11} and S_{21}

Three different values of d are evaluated in order to observe its effects on S_{11}, starting from 3 mm and increasing up to 3.5 mm with a step size of 0.25 mm. The corresponding results of S_{11} and S_{21} are presented in Figures 5a and 5b.

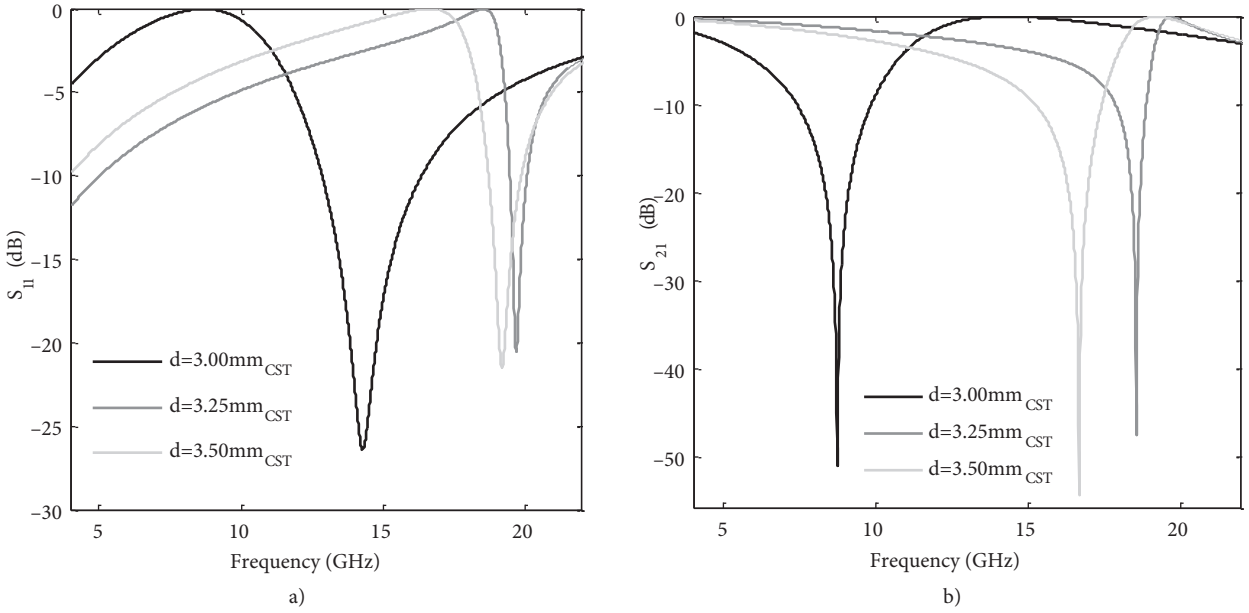

Figure 5. Impact of d on S_{11} ($w = 10$ mm, $t_s = 0.7$ mm, $r = 3$ mm, $\varepsilon_r = 3$ (Rogers 3003), $t_c = 0.035$ mm).

For $d = 3.0$ mm, the S_{11} resonance frequencies are 14.28 GHz and 14.42 GHz for CST and HFSS, respectively. A frequency difference of 0.14 GHz is observed for the corresponding d value, which means the results are pretty close but are not exactly same since the solvers are based on different methods. The increment in d value by 0.25 mm caused a shift in frequency by 5.4 GHz and 5.4 GHz for CST and HFSS, respectively. The corresponding results for each evaluation are presented in Figure 5. As seen in the figure, the return loss values for $d = 3.0$ mm varied between 26.43 dB and 26.02 dB. The mentioned values are 20.57 dB for CST and 19.74 dB for HFSS where $d = 3.25$; for $d = 3.5$ mm the corresponding return loss values are 21.47 and 20.82 dB, respectively.

It is observed that the parameter d has a significant effect on bandwidth. Owing to the results presented the relevant figure, if $d = 3$ the achieved bandwidth is 3.46 GHz by considering the return loss values above 10 dB as the frequency band. For $d = 3.25$ and $d = 3.5$ mm the bandwidth is around 1.15 GHz and 0.61 GHz, respectively.

The comparison results are demonstrated in Table 3 in which the effect of d value is evaluated with respect to the fractional bandwidth values.

As seen in this table the fractional bandwidth varied between 24.3% and 5.2% for S_{11}. The fractional bandwidth achieved was 27.9% for a $d$value of 3 mm.

Table 3. Fractional bandwidth comparison for different d values (w = 10 mm, t_s = 0.7 mm, r = 3 mm, ε_r = 3 (Rogers 3003), t_c = 0.035 mm).

	S_{11}				S_{21}			
d (mm)	f_l (GHz)	f_u (GHz)	f_c(GHz)	BW_f(%)	f_l(GHz)	f_u (GHz)	f_c (GHz)	BW_f(%)
3.00	12.86	16.34	14.3	24.3	7.4	9.84	8.73	27.9
3.25	19.46	19.67	20.5	5.2	17.86	18.87	18.55	5.4
3.50	18.71	19.86	19.18	5.9	15.23	17.41	16.6	13

3.4. Impact of r on S_{11} and S_{21}

In order to analyze the effects of the magnitude of r, a set of simulations are performed and the results are presented in Figure 6.

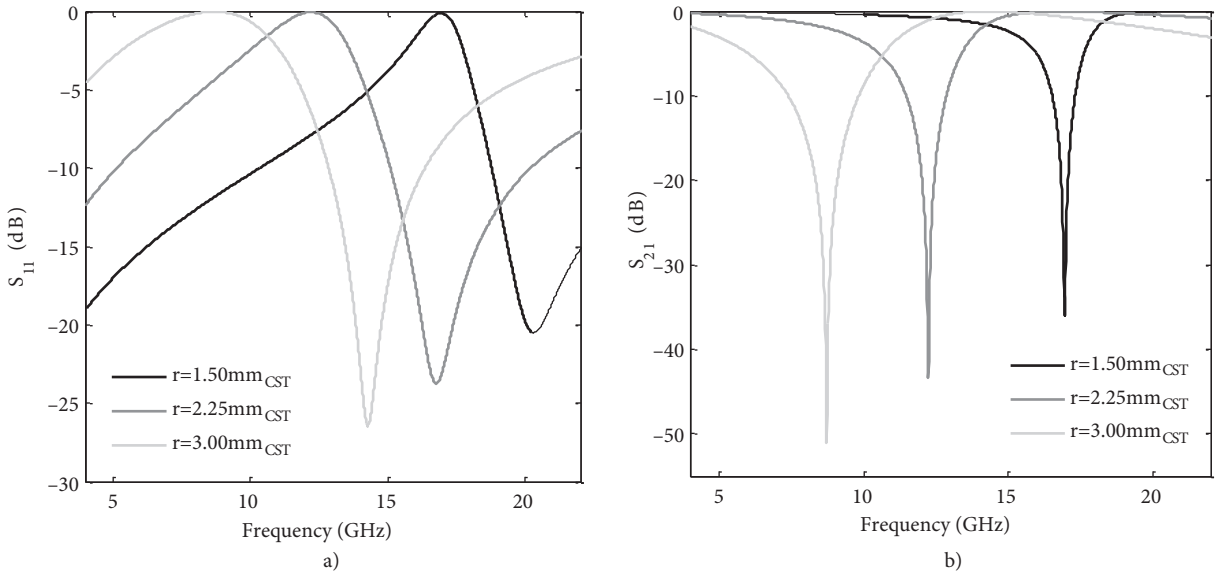

Figure 6. Impact of r on a) S_{11} and S_{21} (w = 10 mm, t_s = 0.7 mm, ε_r = 3 (Rogers 3003), t_c = 0.035 mm).

The increment in the value of r caused a decrement in S_{11} resonance frequency value. The increment in value of$r$ also caused an increment in return loss value. As seen in Figure 6a, the frequency values for r = 1.5 mm are 20.3 GHz (CST) and 20.74 GHz (HFSS) with the return loss values of 20.50 dB and 20.08 dB, respectively. When the r value increased to 2.25 mm, the S_{11} resonance frequency values decreased to 16.76 GHz (CST) and 17.06 GHz (HFSS), whereas the return loss values increased to 23.76 dB (CST) and 23.29 dB (HFSS). The r value is assumed to be 3 mm and in this case again an increment of the frequency by 2.48 GHz (CST) and by 2.61 GHz (HFSS) is observed. On the other hand, return loss increased by 2.67 dB (CST) and 2.69 dB (HFSS) when compared to the condition where r = 2.25 mm.

The impact of r on S_{21} is evaluated for values of 1.5 mm, 2.25 mm, and 3.0 mm and the corresponding results are shown in Figure 6b. The S_{21} values for r = 1.5 mm are 36.04 dB (CST) and 34.88 dB (HFSS) with the corresponding frequencies of 16.96 GHz (CST) and 17.42 GHz (HFSS). The r value increased 0.75 mm and this increment caused a decrement in the S_{21} resonance frequency value (12.24 GHz (CST) and 12.71 GHz (HFSS)). It also caused an increment in insertion loss by a value of 7.38 dB (CST) and 7.14 dB (HFSS) when compared to the values obtained for r = 1.5 mm. For r = 3 mm, the frequencies are 8.73 GHz and 9.12 GHz

with insertion losses of 51.13 dB and 48.95 dB, respectively. To summarize, as seen in Figure 6, the increment in the magnitude of r caused an increment in insertion loss and a reduction in S_{21} resonance frequency value.

3.5. Impact of substrate permittivity (ε_r) on S_{11} and S_{21}

The impact of permittivity values is evaluated for three different substrates. Rogers 3003 ($\varepsilon_r = 3$), Rogers 3006 ($\varepsilon_r = 6.15$), and FR4 ($\varepsilon_r = 4.4$) are used as dielectric layers with different permittivity values and the results are shown in Figure 7.

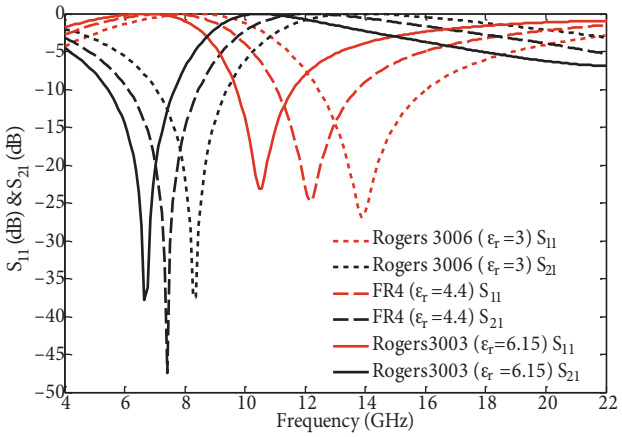

Figure 7. Impact of substrate permittivity on a) S_{11} and b) S_{21} ($w = 10$ mm, $d = 3$ mm, $r = 3$ mm, $t_s = 0.7$ mm, $t_c = 0.035$ mm via CST).

The variation in the permittivity value caused variations in both S_{11} resonance frequency and return loss values. Although no regular change is observed in return loss values, the increment in permittivity value causes a decrement in S_{11} resonance frequency values.

The permittivity value effect on S_{21} evaluated and the results are presented in Figure 7 as well. Similar to the characteristics in S_{11}, the increment in the permittivity value causes a decrement in S_{21} resonance frequency value although there is no such relation in insertion loss values.

Capacitance of an FSS structure varies as a function of thickness of the substrate. Since the increment in the thickness value causes a reduction in the effective permittivity value, it automatically reduces the resonance frequency. As expected, while evaluating the impact of the t_s value, the results satisfactorily agreed with the aforementioned effects. Although thicker substrates cause wider bandwidths it should be noted that in practical uses thicker structures will cause heavier designs.

Permittivity value was another parameter evaluated. As a result higher dielectric constants cause lower resonance frequencies since the structure becomes electrically larger with increasing dielectric constant causing a shift to lower frequencies.

The plate size etched to the dielectric permittivity has a significant effect on determining the resonance frequency. The plate, which is made up of a conductor material, affects the inductance of the unit cell. The parameters that increase the inductivity such as d and r decrease the resonance frequency. As expected, the resonance frequency decreased with the increment of the inductance of the FSS.

3.6. Analysis of the proposed structure with respect to incidence angle

Incidence angle dependency of one of the structures having $w = 10$ mm, $t_s = 0.7$ mm, $d = r$, $\varepsilon_r = 3$ (Rogers 3003), and $t_c = 0.035$ mm is evaluated in terms of angle of incidence. S_{11} and S_{21} characteristics of the structure are presented in Figures 8a and 8b, respectively.

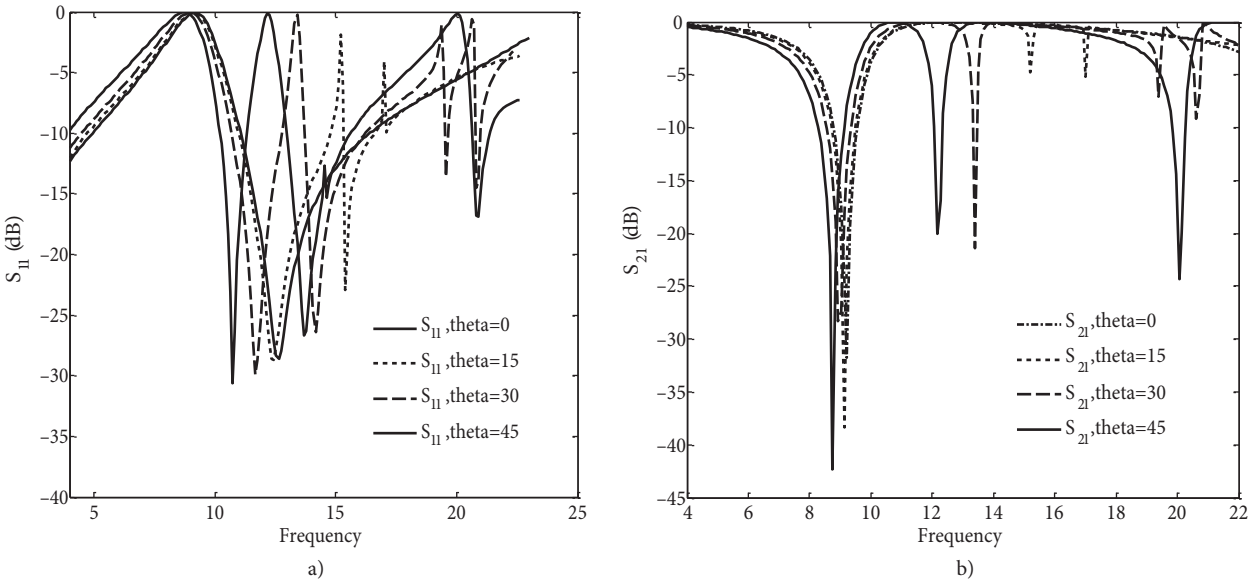

Figure 8. Incidence angle effect t_s on a) S_{11} and b) S_{21} ($w = 10$ mm, $d = 3$ mm, $r = 3$ mm, $t_s = 0.7$ mm, $t_c = 0.035$ mm).

As seen in this figure, the structure has incidence angle dependent characteristics for the angles 15° for S_{11}. The angle of incidence has a negligible effect on S_{21} for 15° , 30° , and 45° , but some unwanted peaks are observed for both evaluations.

4. The proposed FSS structures

S_{11} and S_{21} are two important parameters in order to evaluate the electromagnetic properties of a structure. S_{11} represents the reflection characteristics and S_{21} represents the transmission characteristics. Owing to the parametric analysis results, which are obtained from previous sections, two different FSSs are proposed in order to be used as band-stop filters by considering S_{21}. One of them is a good filter at the C-band, and the other is tuned for use in the X-band. Corresponding data are presented in Table 4. As seen in the table, only the substrate is different when the C-band FSS is compared with the X-band. The X-band FSS has a S_{11} resonance frequency value of 10.79 GHz for CST and 10.46 GHz for HFSS. In order to achieve a wider bandwidth, according to the parametric analyses, the parameter d is determined to have a value of 3 mm. The bandwidth values are 1.86 GHz for the former and 1.82 GHz for the latter. The S_{11} resonance frequency value of the K_u-band for CST is 13.97 GHz with a bandwidth value of 3.44 GHz and for HFSS 13.82 GHz with a bandwidth value of 3.43 GHz.

All the results presented in Table 4 and in previous sections indicate that tunability of the resonance frequency can be achieved via varying the geometrical and material properties of the proposed structure. The structure allows flexibility in C- and X-band operation for band-stop filtering. Not limited to this, the proposed structure can be used as a band-stop filter or a shielding structure in a tunable resonance frequency range that

Table 4. The properties and the results of the proposed FSS geometries.

FSS geometric parameters (mm)	X-band		K_u-band	
Substrate side length (w)	10		10	
Thickness of the substrate (t_s)	0.7		0.7	
Thickness of the conductor (t_c)	0.035		0.035	
Physical size parameter (a)	5.2		5.2	
Separation distances of the bow ties (d)	3		3	
FSS material properties				
Substrate permittivity (ε_r)	6.15		3	
Conductivity of the patch (S/m)	5.8e + 007		5.8e + 007	
Results	CST	HFSS	CST	HFSS
S_{11} resonance frequency (GHz)	10.79	10.46	13.97	13.82
BW (GHz) (S_{11})	1.86	1.82	3.44	3.43
Fractional bandwidth (S_{11})	17.2%	17.3%	24.6%	24.8%
S_{11} return loss (dB)	22.61	23.05	26.8	26.82
S_{21} resonance frequency (GHz)	6.89	6.71	8.61	8.49
BW (GHz) (S_{21})	2.29	2.12	2.40	2.42
Fractional bandwidth (S_{21})	33.2%	32.9%	28.6%	28.3%

includes all frequencies at the C- and X-band. Due to the S_{11} characteristics the structures can be used for radar cross-section reduction as in [14] at X- and K_u-bands with a fractional bandwidth value of 17.2% and 24.6%, respectively. The resonance frequency range that the FSS can be used in as a band-stop filter is determined by considering S_{21} results; meanwhile, according to the parametric analyses the structure can also be used as a shielding structure if the proposed S_{11} results are considered. Among most of the FSS types, which are classified in different groups as [14]–[18], the bandwidth values of the proposed structures are in a satisfactory range for a group 3 type FSS, which are determined as "solid interior or plate types of various shapes" in [1]. The structures are easy to fabricate as compared to the studies such as [16], based on mems technology, and [18], based on loading additional elements such as varactors. The proposed structure has a polarization dependent behavior as expected when compared to the loop type FSS and hybrid FSS models. Although "the solid interior or plate type element is seldom used alone but mostly in conjunction with a "complementary" FSS adjacent to it" [1], they are mostly preferred for creating hybrid structures having larger bandwidth for different polarization types.

5. Conclusion

In this study, we have proposed a new FSS topology and have investigated the effects of the predefined five parameters on insertion loss, resonance frequency, bandwidth, and return loss of the proposed FSS. All the results obtained from the study obtained via two different solvers are validated by means of simulations. As a result of the study, two structures have been proposed for both X- and K_u-bands for RCS reduction. The structures can also be used for C- and X-band applications as band-stop filters. The conclusions can be summarized as follows:

- Depending on the increment in the value of r, an increment in the return loss value and a decrement in the insertion loss value are observed. If all parameters except r remain the same, under the assumption of the double bow-ties located in the center (which means $d = r$) of the FSS, the resonance frequency decreases with the increment in the value of r. Therefore, it can be concluded that by changing r, the frequency can be tuned from K_u-band to X-band operation.

- When d rises, the value of the return loss increases. The increment in d also causes an increment in the resonance frequency.
- Increasing the substrate thickness causes an increment in the value of return loss. Decrements are observed in resonance frequency and insertion loss depending on the increment in the value of t_s.
- Increment in the value of side length of the substrate causes an increment in the value of insertion loss. In contrast to this, when the side length of the substrate increases, return loss and peak frequencies of the return loss and insertion loss decrease.
- Impact of the substrate permittivity has been examined by changing the substrate with the samples of FR4, Rogers 3003, and Rogers 3006. When there is a change from one material to another, which corresponds to a change in permittivity value, both of the return loss and insertion loss oscillate over 20 dB. If a low permittivity substrate is considered when compared to Roger 3006, such as FR4 or Rogers 3003, the peak resonance frequency of S_{21} decreases and it can be tuned to the X-band and even to the C-band.
- Bandwidth is also evaluated and it is concluded that d has a significant effect on bandwidth. The decrement in the value of d causes an increment in bandwidth. Similarly, an increment in bandwidth is observed with a decrement in permittivity. The bandwidth for the proposed K_u-band structure is around 3.44 GHz with a corresponding permittivity value of 3. The bandwidth for the X-band FSS structure is around 1.83 GHz with a corresponding permittivity value of 6.15. In order to make this relation more clear, FR4 having a permittivity value of 4.3 is examined, and a bandwidth value of 2.62 GHz is achieved.

By using the evidence of the parametric analyses, the FSS structure is tuned for operation in X- and K_u-bands with a fractional BW over 20%.

Acknowledgment

This study is made possible by a grant from Ankara University BAP Koordinatörlüğü with grant number 13B4343015. The authors would like to express their gratitude for the relevant support.

References

[1] Munk BA. Frequency Selective Surfaces Theory and Design. New York, NY, USA: Wiley, 2000.

[2] Liang WM, Jun ZS, Qi LF, Wei L, Mei LX, Liang XW. FSS design research for improving the wide-band stealth performance of radar absorbing materials. International Workshop on Metamaterials; 8–10 October 2012; Nanjing China: IEEE. pp. 1-4.

[3] Lee YS, Malek, F, Wee FH. Investigate FSS structure effect on WIFI signal. 5th IET International Conference on Wireless, Mobile and Multimedia Networks (ICWMMN 2013); 22–25 November 2013; Beijing, China: IEEE. pp. 331-334.

[4] Ying M, Kuse, Hori R, Fujimoto T, Seki M, Sato T, Oshima KI. Unit cell structure of AMC with multi-layer patch type FSS for miniaturization. International Symposium on Antennas & Propagation (ISAP), 23–25 October 2013; Nanjing, China: IEEE. pp. 957-960.

[5] Chen HY, Chou YK. An EMI shielding FSS for Ku-band applications. Antennas and Propagation Society International Symposium (APSURSI), 8–14 July 2012; Chicago, IL, USA: IEEE. pp. 1-2.

[6] Barbagallo S, Monorchio A, Manara G. Small periodicity FSS screens with enhanced bandwidth performance. Electron Lett 2006; 42: 382-384.

[7] Azemi, SN, Ghorbani, K, Rowe WST. A reconfigurable FSS using a spring resonator element. Antennas and Wireless Propagation Letters 2013; 12: 781-784.

[8] Zelenchuk D, Fusco V. Split-ring FSS spiral phase plate. Antennas and Wireless Propagation Letters 2013; 12: 284-287.

[9] Yilmaz AE, Kuzuoglu M. Design of square loop frequency selective surfaces with particle swarm optimization via the equivalent circuit model. Radioengineering 2009; 18: 95-102.

[10] Ekici S, Yazgan E. Investigation of transmission and characteristics of frequency selective surfaces. Proceedings of the 13th National Congress on Electrical-Electronics-Computer and Biomedical Engineering; 2009; Ankara, Turkey; pp. 1-3.

[11] Jha KR, Singh G, Jyoti R. A simple synthesis technique of single-square-loop frequency selective surface. Progress in Electromagnetics Research B 2012; 45: 165-185.

[12] Raiva AP, Harackiewicz FJ, Lindsey J. Frequency selective surfaces: design of broadband elements and new frequency stabilization techniques. In Proceedings of the 27th Antenna Application Symposium, 2003; Monticello IL, USA.; IEEE. pp. 17-19.

[13] Can S, Yilmaz AE. Parametric performance analysis of the square loop frequency selective surfaces. Elektrotehniski Vestnik 2013; 80: 110-115.

[14] Edalati A, Sarabandi K. Wideband, wide angle, polarization independent RCS reduction using nonabsorptive miniaturized-element frequency selective surfaces. IEEE T Antenn Propag 2014; 62: 747-754.

[15] Bayatpur F, Sarabandi K. Single-layer high-order miniaturized-element frequency-selective surfaces. IEEE T Microw Theory 2008; 56: 774-781.

[16] Safari M, Shafai C, Shafai L. X-band tunable frequency selective surface using MEMS capacitive loads. IEEE T Antenn Propag 2015; 63: 1014-1021.

[17] AlJoumayly MA, Behdad N. Low-profile, highly-selective, dual-band frequency selective surfaces with closely spaced bands of operation. IEEE T Antenn Propag 2010; 58: 4042-4050.

[18] Sanz-Izquierdo B, Parker EA. Dual polarized reconfigurable frequency selective surfaces. IEEE T Antenn Propag 2014; 62: 764-771.